Avalanche Victim Search via Robust Observers

Nicola Mimmo, Pauline Bernard, and Lorenzo Marconi, *Fellow, IEEE*

***Abstract*— This article deals with the problem of victim localization in avalanches by using controlled unmanned aerial vehicles (UAVs) equipped with an electromagnetic sensor (known as ARVA) typically adopted in these search and rescue scenarios. We show that the nominal ARVA measurement can be linearly related to a quantity that is sufficient to reconstruct the victim position. We explicitly deal with a robust scenario in which the measurement is actually perturbed by the noise that grows with the distance to the victim and propose an adaptive control scheme based on a least-square identifier and a trajectory generator whose role is both to guarantee the persistence of excitation for the identifier and to steer the ARVA receiver toward the victim. We prove that the controller ensures boundedness of trajectories and enables to localize the victim in a domain where the ARVA output is sufficiently informative. We illustrate its performance in a realistic simulation framework specifically developed with real data. The proposed approach could significantly reduce the searching time by providing an exploitable estimate before having reached the victim.**

***Index Terms*— Least-squares identification, nonlinear output feedback, robust observers, search and rescue (S&R) robotics, unmanned aerial vehicles (UAVs).**

I. Introduction

FUTURE search and rescue (S&R) missions will exploit the support of robots more and more extensively. Indeed, robots can boost the already high efficiency of human-based rescue operations while decreasing the risks associated with harsh environments (such as urban disasters, mining accidents, explosions in radiation sites, fires, avalanches, and earthquakes). During the last decades, engineers and scientists developed several aerial robotic solutions, each of them characterized by peculiar abilities and equipped with dedicated sensor suites, to support S&R operations in different disaster areas [1]–[5]. Related to the high mountain environment, Cacace [6], [7] and Bevacqua *et al.* [8] demonstrated how S&R operations can greatly benefit from the use of autonomous unmanned aerial vehicles (UAVs) to survey the environment and collect evidence about the position of a missing person. Furthermore, the European projects SHERPA [9] and AIRBorne [10] address a specific challenge in S&R robotics, i.e., the development of effective technologies and algorithms to support professional alpine rescuer teams in avalanches scenarios.

Within S&R in high mountain, a special role is played by quick localization of buried by avalanches. In these settings, a sensor technology that is typically adopted is the so-called ARVA. The system ARVA consists of two elements: a transmitter and a receiver. The transmitter is worn by the victims and emits an electromagnetic signal detectable by the receiver, which is held by the rescuers. The S&R technique based on the ARVA technology relies on three phases. In the first phase, the rescuers look for the first valid electromagnetic signal. In the second phase, they exploit the ARVA data to find the victim. In the last phase, the rescuers dig to save the buried individual. This article focuses on the automatization of the second phase.

In case of signal detection, the receiver provides information about the electromagnetic field generated by the transmitter sensed at the receiver device location. The rescuers are trained to interpret these data and to move closer to the victim location. Unfortunately, although this technique is common and quite efficient, it requires a nonnegligible amount of time due to the difficulties in walking in avalanche terrains. Furthermore, the rescuers walk on unstable snow with the tangible risk of inducing a second avalanche event. In this context, drones represent a valid alternative to humans. Indeed, if sufficiently smart, ARVA-driven drones can fly autonomously on the snow to find the transmitter location, thus resulting in a faster and safer research.

In principle, there are two main strategies for victim detection. The first is based on following the signal intensity that clearly reaches its maximum on the victim. Techniques falling into this category rely on optimization techniques. The second, on the contrary, is rather based on the design of an observer whose goal is to estimate the transmitter location, without necessarily making the receiver approach the transmitter. The current rescue techniques, along with all the available examples of UAVs equipped with the ARVA technology, belong to the first category [11]–[13]. In fact, those methods belong to the so-called source-seeking control problems, where the agent (or agents in case of collaborative and distributed scenarios) senses the signal emitted by a source located at an unknown position. By the knowledge of this signal, and maybe the agent's position, the control goal is to steer the agent toward the source. Remarkable examples of generic source-seeking applications (not ARVA-grounded) include [14]–[16] in which the extremum-seeking control paradigm has been exploited to

Manuscript received November 15, 2019; revised June 30, 2020; accepted July 29, 2020. Date of publication September 14, 2020; date of current version June 10, 2021. Manuscript received in final form August 11, 2020. This work was supported by the H2020 European Project [Aerial Robotic Technologies for Professional Search and Rescue (AirBorne)] under Grant 780960. Recommended by Associate Editor M. Maggiore. *(Corresponding author: Nicola Mimmo.)*

Nicola Mimmo and Lorenzo Marconi are with the Department of Electrical, Electronic and Information Engineering, University of Bologna, 40136 Bologna, Italy (e-mail: nicola.mimmo2@unibo.it; lorenzo.marconi@unibo.it).

Pauline Bernard is with the Systems and Control Centre, MINES ParisTech, Université PSL, 75006 Paris, France (e-mail: pauline.bernard@mines-paristech.fr).

Color versions of one or more of the figures in this article are available online at https://ieeexplore.ieee.org.

Digital Object Identifier 10.1109/TCST.2020.3016665

1063-6536 © 2020 IEEE. Personal use is permitted, but republication/redistribution requires IEEE permission.
See https://www.ieee.org/publications/rights/index.html for more information.

Authorized licensed use limited to: Universita degli Studi di Roma La Sapienza. Downloaded on July 13,2023 at 11:03:08 UTC from IEEE Xplore. Restrictions apply.

provide the solution in the absence of both a detailed output map and information about the agent's position. Furthermore, Mayhew *et al.* [17] provided a control strategy inspired by a line-search minimization algorithm for unconstrained optimization of nonlinear functions without gradient information, whereas Mellucci *et al.* [18] proposed a gradient-free control law (a sliding mode controller solving a boundary tracking problem), which exploits local measurements of the phenomenon at the vehicle's position only.

The main advantage of these extremum-seeking approaches is that they require very little knowledge of the output map. Typically, only the convexity and the nature of the extremum under investigation must be known to properly set up a minimization or a maximization problem. On the contrary, the observer-based methods rely on the model of the output map to build an estimator. Indeed, when the output map is known and the focus of the problem is the estimation of the plant' state associated with the extremum, such methods allow to obtain a faster estimate without having to drive the plant to this extremum. This feature is crucial in the context of avalanche rescue since it may allow one to save precious time and efforts from the rescuers.

This article presents an algorithm that estimates the victim location by following a trajectory that is sufficiently "rich" in ARVA data. Our first contribution is to show that the ARVA output can be approximated by an output that is linear in a quantity enabling to reconstruct the victim position. It follows that the latter can be estimated by means of a least-square algorithm if the receiver's trajectory is sufficiently exciting [19]. A distinguishing feature of our work is that we explicitly consider the noise corrupting the ARVA signal whose magnitude grows with the relative distance between the transmitter and the receiver. The reference trajectory generator must thus serve a triple purpose: 1) ensuring boundedness of the drone's trajectory; 2) guaranteeing persistence of excitation for estimation of the victim position; and 3) bringing the receiver closer to the victim to limit the noise and improve the estimation. By adopting common terminologies, the approach we follow in this article falls into the adaptive control category and more specifically in the class of the indirect adaptive control in which the plant parameters are estimated online and used to calculate the controller parameters [19]. In this class of problems, the control law cannot be designed independently of the identification scheme. Rather it must accomplish the double role of sufficiently exciting the system to make it sufficiently informative for identification purposes and to use the resulting identification outcome to move closer to the victim [20]–[23]. This article presents an indirect adaptive control algorithm based on a least-squares identifier and a reference trajectory generator whose role is both to guarantee the persistence of excitation for the identifier and to steer the ARVA receiver toward the victim. We show that there exists a region where the ARVA is sufficiently informative to guarantee convergence to a ball around the victim, whose radius depends on the measurement noises and the amplitude of the excitation signal. The advantage of this approach is that it can provide an exploitable estimate of the victim position before having actually reached it.

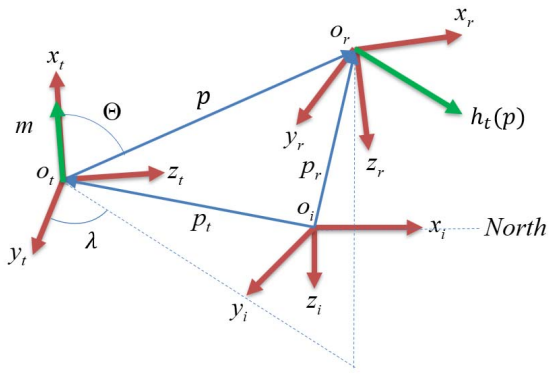

Fig. 1. Reference frames definition.

Moreover, the estimation and control scheme proposed in this work can be applied to any electromagnetic source, which can be modeled as a dipole. Remarkable examples of these sources are the emergency locator transmitters (ELTs) based on omnidirectional radio beacons worldwide used by airplanes and ships. In those contexts, observer-based methods are instrumental to obtain an indication about where to concentrate on the rescue efforts.

The performances of the proposed method are checked in a dedicated, high-fidelity simulator. The simulation environment has been defined by considering both the theoretical model of the system and the data collected using real field experiments in which the ARVA EM field has been sampled and geolocalized to create a 3-D map.

This article is organized as follows. Section II introduces the notation. Then, Section III describes the ARVA system and Section IV presents the blocks constituting the control scheme (i.e., the identifier, the reference trajectory generator, and the plant stabilizer), whereas the main theorem is presented in Section V. Finally, Section VI illustrates the performance of our adaptive control in simulations.

II. Notations

For any $x \in \mathbb{R}^3$, we let $S(x) \in \mathfrak{so}(3)$ be a skew-symmetric matrix and we denote with $^\vee : \mathfrak{so}(3) \mapsto \mathbb{R}^3$ the inverse operator fulfilling $x = (S(x))^\vee$. By $\|\cdot\|$, we denote the standard Euclidean norm and $\|f\|_{t_0,t} = \sup_{s\in[t_0,t]} \|f(s)\|$ for $t \geq t_0 \geq 0$. A function $\gamma : \mathbb{R}_{\geq 0} \to \mathbb{R}_{\geq 0}$ is said to be class-$\mathcal{K}$ if $\gamma(0) = 0$ and γ is strictly increasing. A function $\beta : \mathbb{R}_{\geq 0} \times \mathbb{R}_{\geq 0} \to \mathbb{R}_{\geq 0}$ is said to be class-$\mathcal{KL}$ if for every $s \in \mathbb{R}_{\geq 0}$, $r \mapsto \beta(r, s)$ is class-$\mathcal{K}$, and for every $r \in \mathbb{R}_{\geq 0}$, $s \mapsto \beta(r, s)$ is decreasing and $\lim_{s\to+\infty} \beta(r, s) = 0$. $\mathcal{B}_\rho(x)$ denotes the ball of radius ρ centered at x. Three Cartesian coordinate frames are defined (see Fig. 1): $\mathcal{F}_i = (\mathrm{O}_i, \mathrm{x}_i, \mathrm{y}_i, \mathrm{z}_i)$ indicates the inertial frame with origin O_i, with the unitary vector x_i oriented toward geographic north, z_i oriented opposite to the local gravity vector, and y_i oriented to create a right-hand frame, while $\mathcal{F}_t = (O_t, \mathrm{x}_t, \mathrm{y}_t, \mathrm{z}_t)$ and $\mathcal{F}_r = (\mathrm{O}_r, \mathrm{x}_r, \mathrm{y}_r, \mathrm{z}_r)$ are the body right-hand frames associated to the transmitter worn by the victim and to the receiver installed on the drone. For sake of simplicity, we assume that the body frame of the drone coincides with $\mathcal{F}_r$. The position of O_r relative to O_t is indicated by the vector $p \in \mathbb{R}^3$, with $p = p_r - p_t$, while the positions of O_r and O_t relative to O_i are indicated,

Authorized licensed use limited to: Universita degli Studi di Roma La Sapienza. Downloaded on July 13,2023 at 11:03:08 UTC from IEEE Xplore. Restrictions apply.

respectively, by the vectors $p_r \in \mathbb{R}^3$ and $p_t \in \mathbb{R}^3$. Throughout this article, and only when needed, we shall use the apex i, t, and r on the left of the vectors p, p_t, and p_r to denote the representation of the previous vectors in the reference frames $\mathcal{F}_i$, $\mathcal{F}_t$, and $\mathcal{F}_r$, respectively (for instance, ${}^i p$ denotes a representation of p in $\mathcal{F}_i$). The quantities are intended in the inertial frame $\mathcal{F}_i$ when the left-side apex is not indicated. The rotation matrices from $\mathcal{F}_i$ to $\mathcal{F}_t$ and from $\mathcal{F}_r$ to $\mathcal{F}_i$ are, respectively, denoted by R_t and R_r, whereas the relative rotation from $\mathcal{F}_t$ to $\mathcal{F}_r$ is indicated by R_{rt}.

Definition 1 (Persistence of Excitation [19]): Given $T > 0$, a locally integrable function $\phi : \mathbb{R}_{\geq 0} \mapsto \mathbb{R}^n$ is said to be persistently exciting (PE) if there exists a positive real $\alpha_0 > 0$ such that

$$\frac{1}{T}\int_{t-T}^{t} \phi(\tau)\phi^\top(\tau)\, d\tau \geq \alpha_0 I \quad \forall t \geq T. \tag{1}$$

III. Characterization of the System ARVA

The transceivers commercially available have two working modalities, namely, they can work as receivers or as transmitters, with a manual switch used to commute between the two modes. The ARVA system is based on the emission and sensing of an electromagnetic field. More precisely, the transmitter, worn by the victim, emits a signal that is sensed, elaborated, and made available to the rescuer by the receiver. Before starting their activities, experienced skiers switch the worn sensor to the transmitter mode. In case of accident, companions not buried by the avalanche, or rescuers who reach the disaster area, switch their device in the receiver mode and start searching the victim by following the electromagnetic flux lines. In this paragraph, we go through the main physical principles of the sensor and its main features that are instrumental for the development of the automatic search algorithms presented in Section V.

A. ARVA in the Transmitter Mode

The ARVA system relies on a transmitter device that generates a magnetic field modeled as a dipole aligned with the x_t axis of $\mathcal{F}_t$ with an amplitude $m \in \mathbb{R}_{>0}$. The electromagnetic vector field, described in $\mathcal{F}_t$, is indicated by $h_t \in \mathbb{R}^3$. Denoting (p_x, p_y, p_z) the components of the vector p expressed in $\mathcal{F}_t$ (i.e., ${}^t p = \mathrm{col}(p_x, p_y, p_z)$), a mathematical model of the magnetic vector field at ${}^t p$ is given by (see [24])

$$h_t({}^t p) = \frac{m}{4\pi \|p\|^5} \mathrm{A}_c({}^t p) \tag{2}$$

where

$$\mathrm{A}_c({}^t p) := \begin{bmatrix} 2p_x^2 - p_y^2 - p_z^2 \\ 3p_x p_y \\ 3p_x p_z \end{bmatrix}.$$

The model can also be expressed in polar coordinates $(\Theta, \lambda, \|p\|)$ defined as

$$\begin{bmatrix} \Theta \\ \lambda \\ \|p\| \end{bmatrix} := \begin{bmatrix} \cos^{-1}\left(\dfrac{p_x}{\sqrt{p_x^2 + p_y^2 + p_z^2}}\right) \\ \tan^{-1}(p_z/p_y) \\ \sqrt{p_x^2 + p_y^2 + p_z^2} \end{bmatrix} \tag{3}$$

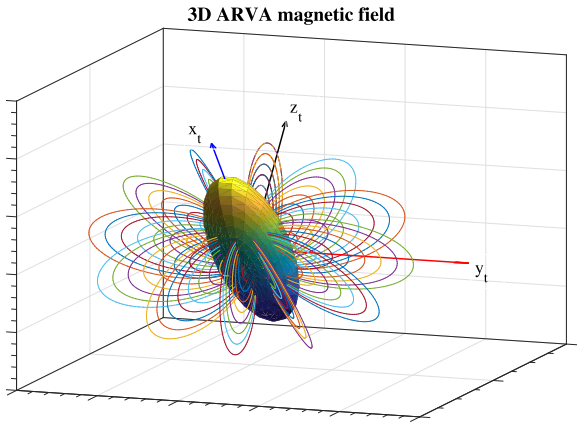

Fig. 2. 3-D representation of flux lines and iso-power surfaces (ellipsoid) for a theoretical magnetic dipole.

thus leading to

$$h_t(\|p\|, \Theta, \lambda) = \frac{m}{4\pi \|p\|^3} \mathrm{A}_p(\Theta, \lambda) \tag{4}$$

where

$$\mathrm{A}_p(\Theta, \lambda) = \begin{bmatrix} 2 - 3\sin^2\Theta \\ 3\cos\Theta \sin\Theta \cos\lambda \\ 3\cos\Theta \sin\Theta \sin\lambda \end{bmatrix}.$$

The intensity of the magnetic field is then obtained from the previous relation (see [24] and Fig. 2)

$$\|h_t\| = \frac{m}{4\pi \|p\|^3}\sqrt{1 + 3\cos^2\Theta}. \tag{5}$$

The flux lines described by (4) are symmetric with respect to the transmitter x-axis and are shown in Fig. 2 (coloured lines). Furthermore, (5) can be exploited to compute the iso-power lines that are also symmetric with respect to the transmitter x-axis. The iso-power lines are plotted in Fig. 2.

Remark 1: The models (2)–(5) do not consider the transmitter rotation with respect to the inertial space because they are written in the transmitter reference frame. Moreover, the burial depth is not clearly highlighted because the snow surface is not specified. As described in [25], typical burial depths of few meters do not disrupt the ideal magnetic dipole here presented. Finally, this article does not need to describe the projection of the ARVA field of the snow surface because the exploited robotic agent is not constrained to move on the ground.

B. ARVA in the Receiver Mode

The ARVA equipment has three antennas directed along the receiver frame axes x_r, y_r, and z_r, namely, along the longitudinal, lateral, and vertical direction of the sensor case, respectively. We assume that the ARVA receiver position p_r and orientation R_r in the inertial frame are known.

The magnetic field read by the receiver, denoted by $h_m(p, R_{rt}, t)$, is given by the projection of the vector h_t onto the $\mathcal{F}_r$ frame corrupted by the sensor noise

$$h_m(p, R_{rt}, t) = R_{rt} h_t({}^t p) + {}^r w(t) \tag{6}$$

where ${}^r w(t) : \mathbb{R} \mapsto \mathbb{R}^3$ indicates the electromagnetic interference (EMI) expressed in the receiver frame. This noise

Authorized licensed use limited to: Universita degli Studi di Roma La Sapienza. Downloaded on July 13,2023 at 11:03:08 UTC from IEEE Xplore. Restrictions apply.

is bounded by a positive constant $\|^r w\|_\infty$. We will denote $h_n(p, R_{rt}) = R_{rt} h_t({}^t p)$ the nominal EM field at the receiver, equal to $h_m(p, R_{rt}, t)$ in absence of noise.

In the following, we exploit the ARVA output (6) to estimate the transmitter's position p_t, namely the victim's position, by means of an observer. The estimation of its orientation R_t is not crucial and is left aside in this article.

1) Toward the Transmitter Position Estimation: The direct design of a nonlinear observer for this system is not straightforward unless adopting an extended Kalman filter [26], which, however, would require linearizing the system and would ensure only a local convergence. On the other hand, the constant nature of the unknowns, namely the position and orientation of the victim, can be exploited for the design of an observer which benefits of more appealing properties (easy design, global stability, and so on). In this context, we manipulate the nonlinear map $h_n(p, R_{rt})$ to find a change of unknowns that makes the output map linear, thus leading to a simpler observer design. In other words, we design an observer by immersion, i.e., by immersing (in the differential geometry sense) the state space into a space of larger dimension [27].

More precisely, (3), computations on h_n show that p, R_t, and h_n fulfill a polynomial equation of the form

$$p^\top M p - (4\pi)^2 \|h_n\|^2 (p^\top p)^4 = 0 \tag{7}$$

in which $e_1 = \mathrm{col}(1, 0, 0)$ and $M = M^\top = m^2(3R_t e_1 e_1^\top R_t^\top + I)$. Equation (7) is a polynomial of degree 8 in the unknown constants $p_t \in \mathbb{R}^3$ and $M \in \mathbb{R}^{3\times 3}$ with coefficients depending on p_r and h_n that are known, modulo some noise on h_n. It could therefore be used as an implicit output map to estimate p_t and M (nine unknowns) by an immersion in a linear space of order 54, but this method is practically unfeasible. Instead, we show that a model approximation leads to a practical solution.

2) ARVA Model Approximation: A detailed analysis of (5) reveals that the complexity is introduced by the term $(1 + 3\cos^2\Theta)^{1/2}$. Therefore, the idea is to approximate this function with an equivalent one, namely $f_{\mathrm{eq}}(\Theta)$, which belongs to the family of functions that are isomorphic to $(1 + 3\cos^2\Theta)^{1/2}$ and make (5) inversely proportional to a polynomial of p. This article adopts this approximation

$$\frac{1}{\sqrt[3]{1 + 3\cos^2\Theta}} \approx \frac{1}{a^2}\cos^2\Theta + \frac{1}{b^2}\sin^2\Theta. \tag{8}$$

The selection of this function is motivated by the fact that the iso-power surface of the electromagnetic field of (4) look like ellipsoids, which are x_t-axial symmetric, and whose shape is defined by a, $b \in \mathbb{R}_{>0}$. Finally, the coefficients a and b are known and chosen to minimize the quadratic error with respect to $(1 + 3\cos^2\Theta)^{-1/3}$. Fig. 3 shows this approximation in a polar graph. Given the approximation of (8) and keeping in mind (3), the norm of h_n becomes

$$\|h_n\| \approx \frac{m}{4\pi}\left(\frac{a^2 b^2}{b^2 p_x^2 + a^2(p_y^2 + p_z^2)}\right)^{\frac{3}{2}} \tag{9}$$

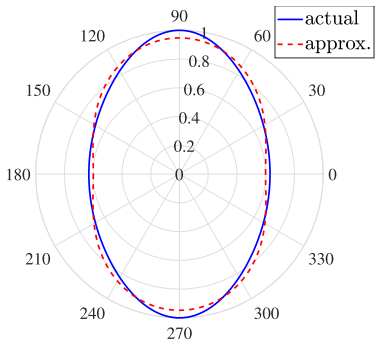

Fig. 3. Polar plot of the function $(1 + 3\cos^2\Theta)^{-1/3}$ (blue line) and its approximation $a^{-2}\cos^2\Theta + b^{-2}\sin^2\Theta$ (red line). The approximation introduces an error that is less than the $\pm 6\%$ of the nominal value.

from which it is possible to obtain the following polynomial function of order 2:

$$\eta = \Phi^\top(p_r)\,\mathrm{x}(x_t) \tag{10}$$

in which

$$\eta = \left(\frac{m}{\|h_n\|4\pi}\right)^{\frac{2}{3}}(ab)^2 \tag{11}$$

$$\Phi(p_r) = \mathrm{col}\big(p_{x_r}^2,\ 2p_{x_r}p_{y_r},\ 2p_{x_r}p_{z_r},\ p_{y_r}^2,\ 2p_{y_r}p_{z_r},\ p_{z_r}^2,\ -2p_{x_r},\ -2p_{y_r},\ -2p_{z_r},\ 1\big) \tag{12}$$

with $p_r = (p_{x_r}, p_{y_r}, p_{z_r})$, are known signals and

$$\mathrm{x}(x_t) = \mathrm{col}(\overline{m}_{11}, \overline{m}_{12}, \overline{m}_{13}, \overline{m}_{22}, \overline{m}_{23}, \overline{m}_{33}, \overline{p}_t, \varrho) \tag{13}$$

is the vector of the unknown constants with $\overline{m}_{ij}$ the entries of $\overline{M} = \overline{M}^\top > 0$, $\overline{p}_t = \overline{M} p_t$, and $\varrho = p_t^\top \overline{M} p_t$ with

$$\overline{M} = R_t\,\mathrm{diag}(b^2, a^2, a^2)R_t^\top. \tag{14}$$

It is worth observing that estimating the constant vector $\mathrm{x}(x_t) \in \mathbb{R}^{10}$ is sufficient to obtain an estimate for p_t. Indeed, the first six components of $\mathrm{x}(x_t)$ give an estimate for $\overline{M}$, whereas $\overline{p}_t$ estimates $\overline{M} p_t$ so that p_t can then be recovered by inversion of $\overline{M}$.

Property 1 (Partial Bijectivity of the Map x*):* The map $\mathrm{x} : \mathbb{R}^3 \times SO(3) \mapsto \mathbb{R}^{n_p}$ is partially invertible with respect to p_t. Namely, there exists a partial left-inverse denoted Υ such that $p_t = \Upsilon \circ \mathrm{x}(p_t, R_t)$ for any $(p_t, R_t) \in \mathbb{R}^3 \times SO(3)$. Furthermore, Υ is globally Lipschitz on $\mathbb{R}^{10}$, i.e., there exists a constant $L > 0$ such that, for any x_1, $\mathrm{x}_2 \in \mathbb{R}^{10}$, $\|\Upsilon(\mathrm{x}_1) - \Upsilon(\mathrm{x}_2)\| \le L\|\mathrm{x}_1 - \mathrm{x}_2\|$.

In practice, such a global inverse of x can be obtained by projection of $\overline{M}$ in the following way. According to (14), $\overline{M}$ has as eigenvalues $\{a^2, a^2, b^2\}$. Therefore, for any $\overline{M} \in \mathbb{R}^{3\times 3}$ and $\overline{p}_t \in \mathbb{R}^3$, we can take $\Upsilon(\mathrm{x}) = (U\,\mathrm{sat}(\Sigma)V^\top)^{-1}\overline{p}_t$, where U, Σ, and $V^\top$ are the elements of the singular value decomposition of $\overline{M}$, such that $U\Sigma V^\top = \overline{M}$ and sat saturates the entries of the diagonal matrix Σ in the interval $[\kappa^{-1}\min(a^2, b^2),\ \kappa\max(a^2, b^2)]$, where $\kappa \ge 1$ represents a tolerance factor.

3) Model Mismatch for the Approximated ARVA: Substituting the real noisy measurement h_m in place of the ideal measurement h_n in the definition (11) of η leads to a new

Authorized licensed use limited to: Universita degli Studi di Roma La Sapienza. Downloaded on July 13,2023 at 11:03:08 UTC from IEEE Xplore. Restrictions apply.

output defined by

$$y_t = \left(\frac{m}{\|h_m\|4\pi}\right)^{\frac{2}{3}}(ab)^2. \tag{15}$$

Now, using a first-order approximation on the noise ${}^r w$, it turns out that

$$y_t = \Phi^\top(p_r)\mathrm{x}(x_t) + \Delta(\|p\|, \Theta) + \nu_t(p_r, x_t, t) \tag{16}$$

where

$$\Delta(\|p\|, \Theta) = \|p\|^2\left[\frac{1}{\sqrt[3]{1+3\cos^2\Theta}} - \frac{1}{a^2}\cos^2\Theta + \frac{1}{b^2}\sin^2\Theta\right]$$

$$\nu_t(p_r, x_t, t) \approx (ab)^2\left(\frac{m}{4\pi}\right)^{\frac{2}{3}}\nabla_A(\Theta, \lambda)\|p\|^5\,{}^r w(t) \tag{17}$$

with $\|\nabla_A(\Theta, \lambda)\|$ bounded.

Property 2 (Model Mismatch in y_t): There exists a class-$\mathcal{K}_\infty$ function γ_t such that the output map y_t of (16) verifies for all $t \geq 0$

$$|\Delta(\|p\|, \Theta) + \nu_t(p_r, x_t, t)| \leq \gamma_t(\|p\|).$$

A detailed analysis of (17) reveals that $\gamma_t(\|p\|) = c\max\{\|p\|^2, \|p\|^5\|{}^r w\|_\infty\}$ for some $c > 0$. As a consequence, the output y_t becomes closer to $\Phi^\top(p_r)\mathrm{x}(x_t)$ (which is proportional to $\|p\|^2$) as p gets closer to zero (i.e., p_r closer to p_t).

C. Receiver Dynamics

The receiver is assumed to be rigidly installed on a quadcopter, whose dynamics is captured by the following model [28]:

$$\begin{cases} \dot{p}_r = v_r \\ m\dot{v}_r = mg + R_r M_F u \\ \dot{R}_r = -R_r S({}^r\omega_r) \\ J\,{}^r\dot{\omega}_r = -S({}^r\omega_r)J\,{}^r\omega_r + M_\tau u \end{cases} \qquad y_r = x_r \tag{18}$$

with state $x_r = (p_r, v_r, R_r, {}^r\omega_r) \in \mathcal{M}_r := \mathbb{R}^3 \times \mathbb{R}^3 \times SO(3) \times \mathbb{R}^3$ denoting the drones position, velocity, orientation, and angular velocity, respectively, input $u \in \mathbb{R}^4_{>0}$ denoting the vector of the propeller speeds, and measurable output $y_r = x_r$. The terms $M_F \in \mathbb{R}^{1\times 4}$ and $M_\tau \in \mathbb{R}^{3\times 4}$ are two known constant matrices.

D. Overall System and Problem Statement

Gathering (16) and (18) and the constant quantities p_t and R_t, we finally get

$$\begin{cases} \dot{p}_t = 0 \\ \dot{R}_t = 0 \\ \dot{p}_r = v_r \\ m\dot{v}_r = mg + R_r e_z M_F u \\ \dot{R}_r = -R_r S({}^r\omega_r) \\ J\,{}^r\dot{\omega}_r = -S({}^r\omega_r)J\,{}^r\omega_r + M_\tau u \end{cases} \tag{19a}$$

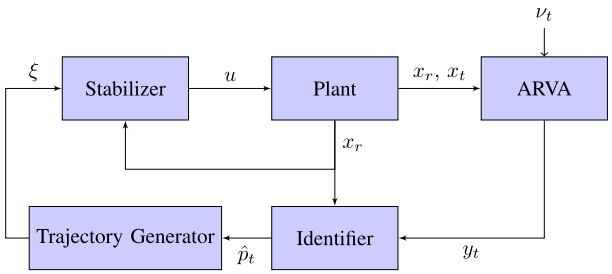

Fig. 4. Representation of the closed-loop system.

with $x_t = (p_t, R_t) \in \mathcal{M}_t := \mathbb{R}^3 \times SO(3)$, $x_r = (p_r, v_r, R_r, \omega_r) \in \mathcal{M}_r$, and outputs $y_t \in \mathbb{R}$ and $y_r \in \mathbb{R}^9$ defined by

$$\begin{aligned} y_t &:= \Phi^\top(p_r)\mathrm{x}(x_t) + \nu_t(p_r, x_t, t) \\ y_r &:= x_r \end{aligned} \tag{19b}$$

with the maps $\mathrm{x} : \mathbb{R}^3 \times SO(3) \to \mathbb{R}^{10}$ and $\Phi : \mathbb{R}^3 \to \mathbb{R}^{10}$ defined in (12) and (13). The goal is now to estimate the position p_t of the victim as precisely as possible. As seen, this reduces to the estimation of the constant $\mathrm{x}(x_t)$, whose observability is inherently linked to the invertibility of the known quantity $\Phi^\top(p_r)$, with the latter intimately connected to a property of persistence of excitation of the signal p_r. Due to the presence of the noise ν_t, the problem can thus be cast as a robust observation problem of the partial state p_r of (19a) from the measured output (19b).

Remark 2: The availability of receivers able to sense multiple constellations of satellite for positioning generally allows to neglect the GPS error in the formulation (19). This is why the drone position x_r is assumed known. If this is not the case, the following can be adapted to handle the measurement noise (see Remark 4).

Remark 3: The observability study of (19) is performed by considering that the state of the receiver x_r, i.e., the position p_r, the speed v_r, the rotation matrix R_r, and the angular speed ω_r, is fully available as output, so we can consider it as a known time-varying quantity. On the other hand, this state appears in the nonlinear output map besides the unknown (but constant) state of the transmitter, represented by x. Thus, the goal is to study the observability, from one single scalar output y_t, of the multidimensional constant state x. Fortunately, this unknown appears in the output equation in affine form and we can apply the linear observability results that, in this case, lead to the necessity of having the term $\Phi^\top(p_r)$ sufficiently exciting to let us observe x. Lemma 1 shows how to design p_r to make $\Phi^\top(p_r)$ sufficiently exciting.

IV. Proposed Solution

Fig. 4 shows the proposed overall control scheme whose elements are detailed in the following.

A. Identifier

The role of the identifier is to provide an estimation of the victim position by properly processing the ARVA signal.

Authorized licensed use limited to: Universita degli Studi di Roma La Sapienza. Downloaded on July 13,2023 at 11:03:08 UTC from IEEE Xplore. Restrictions apply.

This article adopts the recursive least square (RLS) with forgetting factor detailed in [19] and hereafter briefly recalled in its differential version. Given the ARVA measurement y_t verifying (16), the RLS algorithm is given by

$$\begin{cases} \dot{R} = -\rho\, R + \dfrac{\phi\phi^\top}{1+\phi^\top\phi} \\ \dot{Q} = -\rho\, Q - \dfrac{\phi\, y_t}{1+\phi^\top\phi} \\ \dot{\hat{\mathrm{x}}} = -\Gamma(R\hat{\mathrm{x}} + Q) \end{cases} \qquad \hat{p}_t = \Upsilon(\hat{\mathrm{x}}) \tag{20}$$

in which, for easiness of notation, ϕ denotes the known signal $\Phi(p_r)$ of (16), $\rho > 0$ represents the forgetting factor, the matrix $\Gamma = \Gamma^\top > 0$ is a scaling matrix, and the initial conditions of R and Q are taken for instance as $R(0) = I$ and $Q(0) = 0$. If the vector $\Phi(p_r)$ is PE (see Definition 1) and in the ideal case where $y_t = \Phi(p_r)^\top \mathrm{x}(x_t)$, it is a well-known fact [19] that the origin of the estimation error $\hat{\mathrm{x}} - \mathrm{x}(x_t)$ is globally exponentially stable, and therefore, $\lim_{t\to+\infty} \hat{p}_t(t) = p_t$. In the presence of noise ν_t in (16) verifying Property 2, the following can be proved.

*Property 3 (*x*-Identifier):* Assume that Property 2 holds. Consider a signal $t \mapsto p_r(t)$ that is PE in the sense of Definition 1 for some T and α_0 such that $\Phi(p_r)$ is bounded. For any identifier parameters $\rho > 0$ and $\Gamma = \Gamma^\top > 0$, there exist $\mu > 0$ and a class-$\mathcal{KL}$ function β_p such that any trajectory $t \mapsto \hat{p}_t(t)$ of (20) satisfies

$$\|\tilde{\mathrm{x}}(t)\| \le \beta_p(\|\tilde{\mathrm{x}}(t_0)\|, t - t_0) + \mu\gamma_t(\|p\|_{t_0,t}) \tag{21}$$

for all $t \ge t_0$, with $\tilde{\mathrm{x}} := \hat{\mathrm{x}} - \mathrm{x}(x_t)$ the estimation error.

Proof: The solutions $R(t)$ and $Q(t)$ to (20) are

$$\begin{aligned} R(t) &= e^{-\rho(t-t_0)}\mathrm{I} + \int_{t_0}^{t} \mathrm{e}^{-\rho(\mathrm{t}-\tau)} \frac{\phi(\tau)\phi^\top(\tau)}{1+\phi^\top(\tau)\phi(\tau)}\mathrm{d}\tau \\ Q(t) &= \int_{t_0}^{t} e^{-\rho(t-\tau)} \frac{\phi(\tau)(\phi^\top(\tau)\mathrm{x} + \nu_t)}{1+\phi^\top(\tau)\phi(\tau)} d\tau \\ &= \mathrm{x}e^{-\rho(t-t_0)} - R(t)\mathrm{x} \\ &\quad - \int_{t_0}^{t} e^{-\rho(t-\tau)} \frac{\phi(\tau)\nu_t}{1+\phi^\top(\tau)\phi(\tau)} d\tau. \end{aligned} \tag{22}$$

By considering the positive-definite candidate Lyapunov function $V(\tilde{\mathrm{x}}) = (1/2)\,\tilde{\mathrm{x}}^\top\Gamma^{-1}\tilde{\mathrm{x}}$, its time derivative fulfills

$$\begin{aligned} \dot{V} &= \tilde{\mathrm{x}}^\top\Gamma^{-1}\dot{\tilde{\mathrm{x}}} \\ &= -\tilde{\mathrm{x}}^\top(R\hat{\mathrm{x}} + Q) \\ &= -\tilde{\mathrm{x}}^\top\left(R\tilde{\mathrm{x}} - \int_{t_0}^{t} e^{-\rho(t-\tau)} \frac{\phi(\tau)\nu_t}{1+\phi^\top(\tau)\phi(\tau)} d\tau \right. \\ &\qquad \left. + \mathrm{x}e^{-\rho(t-t_0)}\right). \end{aligned} \tag{23}$$

Since $R(t) \ge 0$ for all t and using Property 2

$$\begin{aligned} \dot{V} &\le -\|\tilde{\mathrm{x}}\|^2\underline{\sigma}(R) + \mathrm{x}e^{-\rho(t-t_0)}\|\tilde{\mathrm{x}}\| \\ &\quad + \|\tilde{\mathrm{x}}\| \int_{t_0}^{t} e^{-\rho(t-\tau)} \frac{\|\phi(\tau)\|\|\nu_t\|}{1+\phi^\top(\tau)\phi(\tau)} d\tau \\ &\le -\|\tilde{\mathrm{x}}\|^2\underline{\sigma}(R) + \mathrm{x}e^{-\rho(t-t_0)}\|\tilde{\mathrm{x}}\| \\ &\quad + \|\tilde{\mathrm{x}}\| \int_{t_0}^{t} e^{-\rho(t-\tau)} \frac{\|\phi(\tau)\|}{1+\phi^\top(\tau)\phi(\tau)} \gamma_t(\|p(\tau)\|) d\tau \\ &\le -\|\tilde{\mathrm{x}}\|^2\underline{\sigma}(R) + \mathrm{x}e^{-\rho(t-t_0)}\|\tilde{\mathrm{x}}\| \\ &\quad + \|\tilde{\mathrm{x}}\|\gamma_t(\|p\|_{t_0,t}) \frac{1}{2\rho}(1 - e^{-\rho(t-t_0)}) \\ &\le -\|\tilde{\mathrm{x}}\|^2\underline{\sigma}(R) + \frac{1}{2\rho}\|\tilde{\mathrm{x}}\|\gamma_t(\|p\|_{t_0,t}) + \mathrm{x}e^{-\rho(t-t_0)}\|\tilde{\mathrm{x}}\|. \end{aligned} \tag{24}$$

For $t \in [t_0, t_0 + T]$, $R(t) \ge R(t_0)e^{-\rho T}$. For $t \ge t_0 + T$, denoting ϕ_m an upper bound of $\|\Phi(p_r)\|$

$$R(t) \ge \int_{t-T}^{t} e^{-\rho(t-\tau)} \frac{\phi(\tau)\phi^\top(\tau)}{1+\phi^\top(\tau)\phi(\tau)} d\tau \ge e^{-\rho T} \frac{\alpha_0 T}{1+\phi_m^2}\mathrm{I}.$$

Therefore, denoting $\alpha_1 = e^{-\rho T}\min\{(\alpha_0 T/(1+\phi_m^2)), \underline{\sigma}(R(t_0))\}$

$$\dot{V} \le -\alpha_1\|\tilde{\mathrm{x}}\|^2 + \frac{1}{2\rho}\|\tilde{\mathrm{x}}\|\gamma_t(\|p\|_{t_0,t}) + \mathrm{x}e^{-\rho(t-t_0)}\|\tilde{\mathrm{x}}\|$$

which gives the required ISS property. In particular, the gain μ of (21) is defined as $\mu := (2\rho\alpha_1)^{-1}$.

Remark 4: If the GPS errors are not negligible, i.e., p_r is not known exactly, more sophisticated schemes can be adopted in place of the least squares, such as a Kalman filter and errors in variables algorithms. These approaches allow to model the positioning inaccuracy as a covariance matrix affecting the process and the regressor. On the other hand, in practice, least squares can still be used by filtering more the p_r data and making them more robust. To do this, we decrease the value of ρ and increase the value of the excitation amplitudes A_i, which will be described in Section IV-B.

B. Reference Trajectory Generator

In order to use the identifier defined earlier, we need $\Phi(p_r)$ bounded and PE, and $p = p_r - p_t$ becoming sufficiently small to reduce the impact of the noise on the estimation error $\tilde{\mathrm{x}}$. The idea is therefore to make p_r follow a reference trajectory ξ composed of an exciting part ξ_e and a "slow" part ξ_s steering p_r to p_t, i.e., reducing p. In order to guarantee boundedness of trajectories, we saturate the slow component ξ_s outside a bounded region where the victim is known to be. More precisely, assume that we know scalars $\underline{b}_i$, $\overline{b}_i$, $i = 1, 2, 3$, such that

$$\underline{b}_i \le p_{t,i} \le \overline{b}_i \quad i = 1, 2, 3$$

and consider any increasing C^2 map $\mathrm{sat} : \mathbb{R}^3 \to \mathbb{R}^3$ such that $\mathrm{sat}(p) = (\mathrm{sat}_1(p_1), \mathrm{sat}_2(p_2), \mathrm{sat}_3(p_3))$ with

$$\mathrm{sat}_i = \begin{cases} \underline{b}_i - \epsilon, & \text{on } (-\infty, \underline{b}_i - \epsilon] \\ \mathrm{Id}, & \text{on } [\underline{b}_i, \overline{b}_i] \\ \overline{b}_i + \epsilon, & \text{on } [\overline{b}_i + \epsilon, +\infty). \end{cases}$$

Authorized licensed use limited to: Universita degli Studi di Roma La Sapienza. Downloaded on July 13,2023 at 11:03:08 UTC from IEEE Xplore. Restrictions apply.

Then, for $i = 1, 2, 3$, let $A_i > 0$ and $\varpi_i > 0$ be such that $\varpi_i \neq \varpi_j$, $i \neq j$. The reference trajectory generator is then represented by a dynamic system described by the following equations:

$$\dot{\xi}_s = f_s(\hat{p}_t - \xi_s), \quad \xi = \text{sat}(\xi_s) + \xi_e \tag{25a}$$

with $\xi_s(t_0) = p_r(t_0)$

$$\xi_e(t) = \begin{pmatrix} A_1 \sin \varpi_1 t \\ A_2 \sin \varpi_2 t \\ A_3 \sin \varpi_3 t \end{pmatrix} \tag{25b}$$

and where $f_s(\cdot)$ is defined as

$$f_s(\upsilon) = f_{s,\max} \frac{K\|\upsilon\|}{\sqrt{1 + K^2\|\upsilon\|^2}} \frac{\upsilon}{\|\upsilon\|} \tag{26}$$

with $K > 0$. Note that $f_s(\cdot)$ is continuous on $\mathbb{R}^3$, globally bounded by $f_{s,\max}$, such that $f(0) = 0$ and $f_s(\upsilon)$ has the direction of υ.

The previous reference signal generator is justified by the "dual control" objective that characterizes the problem, namely exciting the system to identify the victim position and moving closer to the victim to have a better signal-to-noise ratio. The interplay between the two actions is managed by imposing two time scales, which are enforced by reducing the parameter $f_{s,\max}$. In fact, the following can be proved.

Lemma 1: For any A_i and ϖ_i defined as above, the signal ξ_e defined in (25) is such that $\Phi(\xi_e)$ is bounded and PE, and there exist $f^\star_{s,\max} > 0$ and $\varepsilon > 0$ such that for all positive $f_{s,\max} \leq f^\star_{s,\max}$ and for any tracking error $t \mapsto e(t)$ bounded by ε, with $e := p_r - \xi$, $\Phi(\xi_e + \text{sat}(\xi_s) + e)$ is also bounded and PE.

The rest of this section is dedicated to the proof of Lemma 1.

1) $\Phi(\xi_e)$ Is Bounded and PE With Level $\alpha^\star_0$: The vector $\Phi(p_r)$ is composed of terms such as ξ_{e_i}, $\xi^2_{e_i}$, and $\xi_{e_i}\xi_{e_j}$ with $i \neq j$ and is thus bounded. Exploiting the Werner's formulas, it is possible to write the following relations:

$$\begin{aligned} \xi^2_{e_i} &= \frac{A_i^2}{2} - \frac{A_i^2}{2}\cos(2\varpi_i t) \\ \xi_{e_i}\xi_{e_j} &= \frac{A_i A_j}{2}(\cos((\varpi_i - \varpi_j)t) - \cos((\varpi_i + \varpi_j)t)). \end{aligned} \tag{27}$$

From (12), defining the column vector $\bar{\omega}$ as

$$\bar{\omega} = \begin{bmatrix} \cos(2\varpi_1 t) \\ \cos(2\varpi_2 t) \\ \cos(2\varpi_3 t) \\ \cos((\varpi_1 - \varpi_2)t) - \cos((\varpi_1 + \varpi_2)t) \\ \cos((\varpi_1 - \varpi_3)t) - \cos((\varpi_1 + \varpi_3)t) \\ \cos((\varpi_2 - \varpi_3)t) - \cos((\varpi_2 + \varpi_3)t) \\ \sin(\varpi_1 t) \\ \sin(\varpi_2 t) \\ \sin(\varpi_3 t) \\ 1 \end{bmatrix} \tag{28}$$

we have $\Phi = F_A F \bar{\omega}$, where

$$F_A = \begin{bmatrix} F_{11} & 0 & 0 & 0 \\ 0 & F_{22} & 0 & 0 \\ 0 & 0 & F_{33} & 0 \\ 0 & 0 & 0 & 1 \end{bmatrix} \tag{29}$$

with

$$\begin{aligned} F_{11} &= -\text{diag}\left(\frac{A_1^2}{2}, \ldots, \frac{A_3^2}{2}\right) \\ F_{22} &= \text{diag}(A_1A_2, \ldots, A_2A_3) \\ F_{33} &= -2\text{diag}(A_1, \ldots, A_3). \end{aligned}$$

and F a constant invertible matrix such that $F_{ij} = \pm 1$. Since $A_i \neq 0$ for $i = 1, 2, 3$, the matrix F_A is nonsingular.

The linear term in (16), i.e., $\Phi^\top(p_r)\text{x}(x_t)$ with $p_r = \xi_e$, can be written as

$$\Phi^\top(\xi_e)\text{x}(x_t) = (F_A F \bar{\omega})^\top \text{x}(x_t) = \bar{\omega}^\top F_A^\top F^\top \text{x}(x_t). \tag{30}$$

The selection of $\varpi_1 \neq \varpi_2 \neq \varpi_3 \neq 0$ ensures that the signal $\bar{\omega}$ contains nine different frequencies, thus guaranteeing the PE property of $\bar{\omega}$ [19], i.e., there exist $T > 0$ and $\alpha_\varpi > 0$ such that

$$\frac{1}{T}\int_{t-T}^{t} \bar{\omega}(\tau)\bar{\omega}^\top(\tau)d\tau \geq \alpha_\varpi I.$$

Therefore,

$$\begin{aligned} &\int_{t-T}^{t} \Phi(\xi_e(\tau))\Phi^\top(\xi_e(\tau))d\tau \\ &\quad = \int_{t-T}^{t} F_A F \bar{\omega}(\tau)\bar{\omega}^\top(\tau)F^\top F_A^\top d\tau \\ &\quad = F_A F \int_{t-T}^{t} \bar{\omega}(\tau)\bar{\omega}^\top(\tau)d\tau F^\top F_A^\top \\ &\quad \geq T\alpha_\varpi F_A F F^\top F_A^\top \\ &\quad \geq T\nu\alpha_\varpi \min_{i,j}\left\{\frac{A_iA_j}{2}, 2A_i, 1\right\}^2 I \end{aligned}$$

with $\nu > 0$ the smallest eigenvalue of $FF^\top$, independent of the A_i and ϖ_i. We thus denote in the following $\alpha^\star_0 = \nu\alpha_\varpi \min_{i,j}\{(A_iA_j/2), 2A_i, 1\}^2$.

2) Effects of a Perturbation δ on the PE: Let us assume that a perturbation δ affects the nominal exciting trajectory ξ_e, namely, $p_r(t) = \xi_e(t) + \delta(t)$. First, if δ is bounded, then $\Phi(p_r)$ is still bounded. Then, the PE level of $\Phi(p_r)$ is affected by the disturbance $\delta(t)$ as follows:

$$\begin{aligned} &\frac{1}{T}\int_{t-T}^{t} \Phi(p_r(\tau))\Phi^\top(p_r(\tau))d\tau \\ &\quad = \frac{1}{T}\int_{t-T}^{t} \Phi(\xi_e(\tau))\Phi^\top(\xi_e(\tau))d\tau + \Delta(t) \\ &\quad \geq \left(\alpha^\star_0 + \underline{\sigma}(\Delta(t))\right)I \end{aligned}$$

with

$$\begin{aligned} \Delta(t) = \frac{1}{T}\int_{t-T}^{t} &\tilde{\phi}(\tau)\Phi(\xi_e(\tau))^\top \\ &+ \Phi(\xi_e(\tau))^\top\tilde{\phi}(\tau) + \tilde{\phi}(\tau)\tilde{\phi}(\tau)^\top d\tau \end{aligned}$$

where $\tilde{\phi}(\tau) = \Phi(p_r(\tau)) - \Phi(\xi_e(\tau))$ has its norm going to zero when $|\delta|$ goes to 0. Using that $\Phi(\xi_e(\tau))$ is bounded, there exists $\delta^\star$ such that for any t and any $|\delta| \leq \delta^\star$, $|\underline{\sigma}(\Delta(t))| < \alpha^\star_0$ and $\Phi(p_r)$ is PE. This shows that a sufficiently small perturbation of ξ_e preserves the PE property with $0 < \alpha_0 < \alpha^\star_0$.

Authorized licensed use limited to: Universita degli Studi di Roma La Sapienza. Downloaded on July 13,2023 at 11:03:08 UTC from IEEE Xplore. Restrictions apply.

The second step consists in showing that the PE is also preserved when δ bounded and sufficiently slow. Assume

$$|\dot{\delta}(t)| \leq f_{s,\max} \quad \forall t.$$

Then, we have for all $\tau \in [t-T, t]$,

$$\Phi(p_r(\tau)) = \Phi(\xi_e(\tau) + \delta(\tau)) = \Phi(\xi_e(\tau) + \delta(t) + \delta(\tau) - \delta(t))$$

with $|\delta(\tau) - \delta(t)| \leq f_{s,\max} T$. Therefore, for all $\tau \in [t-T, t]$,

$$\Phi(p_r(\tau)) = F_m(t)\bar{w}(\tau) + \tilde{\phi}(\tau)$$

with $|\tilde{\phi}(\tau)|$ arbitrarily small if $f_{s,\max}$ is sufficiently small, and $F_m(t) = F_A F + \tilde{F}(t)$ with

$$\tilde{F}(t) = \begin{bmatrix} 0 & 0 & \tilde{F}_{13}(t) & \tilde{F}_{14}(t) \\ 0 & 0 & \tilde{F}_{23}(t) & \tilde{F}_{24}(t) \\ 0 & 0 & 0 & \tilde{F}_{34}(t) \\ 0 & 0 & 0 & 0 \end{bmatrix}.$$

$F_m(t)$ is still invertible for all t, and thus, $F_m(t)F_m(t)^\top$ is still positive definite. Since $\tilde{\phi}$ can be made arbitrarily small, it does not impact the PE as proved above. Besides, since

$$\frac{1}{T}\int_{t-T}^{t} F_m(t)\bar{w}(\tau)\bar{w}^\top(\tau)F_m^\top(t)d\tau \geq \alpha_\varpi F_m(t)F_m^\top(t)$$

we just have to prove that the positive-definite matrix $F_m(t)F_m^\top(t)$ can be lower bounded uniformly in time. We have for all t

$$\det\left(F_m(t)F_m^\top(t)\right) = \det\left(F_A F F^\top F_A^\top\right)$$

so the product of all eigenvalues is constant. Therefore, the only way the minimal eigenvalue could go to zero would be for the maximal one to diverge. However, this is impossible since δ (and thus F_m) is bounded. Therefore, the PE is preserved.

To conclude, since $\text{sat}(\xi_s)$ is bounded with a derivative bounded by $f_{s,\max}$ and e is bounded by ε, $\Phi(\xi_e + \text{sat}(\xi_s) + e)$ is bounded and PE for $f_{s,\max}$ and ε sufficiently small.

Remark 5: It is worth noting that according to Property 3, the estimation error $\tilde{\text{x}}$ is minimized if the parameter μ in (21) is minimized. The proof of Lemma 1 shows that μ can be minimized by maximizing the quantity $e^{-\rho T}(\rho T \alpha_0/\phi_m)$, i.e., by taking $R(t_0)$ with sufficiently large eigenvalues. Since the perturbation impact can be reduced by taking $f_{s,\max}$ and ε sufficiently small, the choice of A_i and ϖ_i is intended to maximize the term $e^{-\rho T}(\rho T \alpha_0^\star/\phi_m)$, i.e.,

$$e^{-\rho T}\rho T \frac{\nu \alpha_\varpi \min_{i,j}\left\{\frac{A_i A_j}{2}, 2A_i, 1\right\}^2}{1 + (\max_{i,j}\{2A_i A_j, 2A_i, 1\} + \max\{|\overline{b}_i|, |\underline{b}_i|\} + \varepsilon)^2}.$$

Then, once T, ϖ_i, and ρ have been designed to maximize $e^{-\rho T}\rho T \alpha_\varpi$, the largest A_i, which ensures $\min_{i,j}\{(A_i A_j/2), 2A_i, 1\}^2 = 1$, represents the best choice.

C. Stabilizer

We do not present a specific low-level control structure of the drone since many solutions already available in the literature could be used (see [28] and citations therein). Rather, we focus on the main property required to the low-level controller in order to have the whole solution properly working.

Property 4 (Controller): For all $\varepsilon > 0$ and for all reference signal $t \mapsto \xi(t)$ generated as in Section IV-B, there exists a control law of the form

$$u = f_\varepsilon(x, \xi) \tag{31}$$

such that the resulting closed-loop tracking error $e := p_r - \xi$ satisfies

$$\|e(t)\| \leq \beta_e(e(0), t - t_0) + \varepsilon \tag{32}$$

for all $t \geq 0$.

The envisioned controller (31) is a static state-feedback controller although dynamic output feedback solutions could be considered in case the state is not fully known. Property (32) asks for practical tracking with a sufficiently small asymptotic bound on the error. The value of ε will be asked to be sufficiently small in Section V to guarantee convergence of the whole control scheme. We emphasize that the existing high-gain solutions (see [28] among the others) could be adopted to have this property fulfilled robustly with respect to system uncertainties. Details about the way such a controller can be constructed are given in Section VI.

Note that since the reference trajectory can be initialized at $\xi(0) = p_r(0)$, the transient can be neglected and we directly assume in the following that the tracking error is bounded by the parameter ε.

V. Main Result

We now analyze the stability of the whole interconnection shown in Fig. 4. The following theorem claims that if the time scales of the references ξ_e and ξ_s are sufficiently different (namely if $f_{s,\max}$ is taken sufficiently small in relation to the ϖ_is), then the estimation error of the victim position practically converges to zero with a practical region that is affected by the amplitude of the exciting signal. Such property, indeed, holds as long as the receiver remains sufficiently close to the victim in relation to the noise features.

Theorem 1: Let the identifier and the reference signal be fixed as in Sections IV-A and IV-B. Furthermore, let the stabilizer be fulfilling Property 4. There exist $f_{s,\max}^\star > 0$ and $\varepsilon > 0$ such that if $f_{s,\max} \leq f_{s,\max}^\star$, there exists a class-$\mathcal{K}$ function γ such that any trajectory of (19), (20), (25), and (31) is bounded and verifies

$$\limsup_{t\to\infty} \|p_r(t) - p_t(t)\| + \|\hat{p}_t(t) - p_t(t)\| \leq \gamma\left(\|\xi_e\|_\infty + \varepsilon\right) \tag{33}$$

as long as $p_r \in \mathcal{B}_{\rho^\star}(p_t)$, with

$$\rho^\star = \min\left\{\left(\frac{1}{cc'\mu L}\right)^{\frac{1}{2}}, \left(\frac{1}{cc'\mu L\|^r w\|_\infty}\right)^{\frac{1}{4}}\right\}$$

where $c' > 0$, and L, c, and μ denote the Lipschitz constant appearing in Property 1, the noise gain in γ_t defined in Property 2, and the ISS parameter of x-identifier appearing in Property 3, respectively.

The boundedness of all trajectories, guaranteed by the saturation of ξ_s, ensures that the drone remains in a predefined zone containing the avalanche area. The size of this region

Authorized licensed use limited to: Universita degli Studi di Roma La Sapienza. Downloaded on July 13,2023 at 11:03:08 UTC from IEEE Xplore. Restrictions apply.

depends on the chosen saturation, the amplitude of the excitation, and the tracking performance ε of the controller.

We observe that due to the persistent excitation, we cannot ensure $p_r = p_t$ asymptotically, and from Property 2, the noise ν_t does not completely disappear, producing a residual error on the estimation depending on the size of γ_t.

The size of the region $\mathcal{B}_{\rho^\star}(p_t)$ which guarantees stability and nice asymptotic properties increases when either the amplitude of the noise $\|^r w\|_\infty$ or the parameter μ decreases.

The design degree of freedom that could be used to enlarge the radius $\rho^\star$ is the amplitude of the exciting signal, i.e., A_i with $i = 1, 2, 3$, through the parameter μ as described in Section IV-B. However, according to Property 3, reducing A_i reduces the asymptotic effect of the noise $^r w$ on the estimation error $\tilde{\mathrm{x}}$. Therefore, unfortunately, a reduction of the amplitudes A_i leads both to a reduction of the asymptotic norm of $\tilde{\mathrm{x}}$ and to a reduction of the stability domain. Therefore, there exists a design compromise between the stability requirement and the asymptotic performance.

Remark 6: At first sight, Theorem 1 may look like a local result with little advantage with respect to an EKF. However, the region of attraction is here only to guarantee the stability of the interconnection between the observer and the reference generator, in order to drive the distance to the victim, and thus the noise, to zero. It is important to note that the least-square observer on its own is globally stable and ISS with respect to the noise in all circumstances. In particular, if the gain of the noise is small, the observer may still rapidly provide a reliable estimate of the victim's position, even outside of $\mathcal{B}_{\rho^\star}(p_t)$. On the other hand, using an EKF for the observation of the nonlinear plant would lead to a double locality constraint: remaining in the local convergence region of the EKF (in spite of the noise), besides guaranteeing contraction with the reference generator to bring the noise to zero. It is possible that the noise and the nonlinearities destabilize the observer without leaving a chance to the reference generator to drive the drone closer to the victim.

Remark 7: The fact that the observer is able to provide a workable estimate of the victim's position before actually reaching the victim constitutes a great advantage in the context of avalanche rescuing compared with extremum-seeking methods. This may seem paradoxical since the goal of the rescue team is eventually to reach the victim. However, actually, with an early estimate provided by a fast drone, the rescuers can go early and directly to the victim, thus saving up efforts and time in a very hostile environment. Besides, the observer provides an estimation of the burial depth that the extremum-seeking cannot provide. Finally, the potentiality of this method is enhanced when considering the possibility of estimating the position of multiple victims at the same time. Indeed, each ARVA receiver is able to track four independent transmitters. If the victims are not too far apart, the reference trajectory computed by the observer-tracking scheme for one victim also enables to reduce the noise for the other victims and parallel observers can then provide a reliable estimate for all victims' positions at the same time. On the contrary, any policy based on the extremum-seeking should steer the drone to each transmitter, one per time, with a huge time expense.

The rest of the section provides the proof of Theorem 1 by exploiting the definition of the errors depicted in Fig. 5. First, according to Lemma 1, $\Phi(p_r) = \Phi(\xi_e + \mathrm{sat}(\xi_s) + e)$ is PE for $f_{s,\max}$ and ε sufficiently small.

A. Dynamics of $\tilde{\mathrm{x}}$ as a Function of s and e

The dynamics of $\tilde{\mathrm{x}}$ is described by

$$\|\tilde{\mathrm{x}}(t)\| \leq \beta_p(\|\tilde{\mathrm{x}}(t_0)\|, t - t_0) + \mu\gamma_t(\|p\|_{t_0,t}). \tag{34}$$

On the other hand, the distance p is linked to e as follows:

$$p = (p_r - \xi_e - \mathrm{sat}(\xi_s)) + (\mathrm{sat}(\xi_s) - p_t) + \xi_e = s + e + \xi_e$$

with norm thus bounded by

$$\|p\| \leq \|s\| + \|e\| + \|\xi_e\| \tag{35}$$

because $\|\mathrm{sat}(\xi_s) - p_t\| \leq \|\xi_s - p_t\|$ by definition of the saturation. Using $\gamma_t(\|p\|) = c\|^r w\|_\infty \|p\|^5$ and the inequality $(a+b)^5 \leq 2^4(a^5 + b^5)$ for any $a, b \geq 0$, the substitution of (35) into (34) leads to

$$\begin{aligned}\|\tilde{\mathrm{x}}(t)\| \leq{}& \beta_p(\|\tilde{\mathrm{x}}(t_0)\|, t - t_0) + c'\mu\gamma_t(\|s\|_{t_0,t}) \\ &+ c'\mu\gamma_t(\|e\|_{t_0,t} + \|\xi_e\|_{t_0,t})\end{aligned} \tag{36}$$

for some positive c'.

B. Dynamics of s as a Function of $\tilde{\mathrm{x}}$

The system generating the error s is described by the following differential equation:

$$\dot{s} = f_{s,\max} K \frac{\tilde{p}_t - s}{\sqrt{1 + K^2\|\tilde{p}_t - s\|^2}}. \tag{37}$$

By taking $V = s^\top s$ as a possible Lyapunov function, it turns out that

$$\dot{V} = \dot{s}^\top s + s^\top \dot{s} = \frac{2 f_{s,\max} K}{\sqrt{1 + K^2\|\tilde{p}_t - s\|^2}}\left(\tilde{p}_t^\top s - s^\top s\right) \tag{38}$$

which is negative if $\tilde{p}_t^\top s < s^\top s$. Therefore, (37) is ISS with unitary asymptotic gain, namely, for all $t \geq t_0$

$$\|s(t)\| \leq \beta_s(\|s(t_0)\|, t - t_0) + L\|\tilde{\mathrm{x}}\|_{t_0,t}. \tag{39}$$

C. Interconnection Conditions

The application of the small gain theorem [29] to the interconnection (36)–(39), depicted in Fig. 6, leads to the contraction condition

$$c' L \mu \gamma_t(\cdot) < \mathrm{Id} \tag{40}$$

which, if fulfilled, leads to the conclusion that the system (36)–(39) is ISS with respect to the inputs e and ξ_e, i.e., there exist a $\mathcal{KL}$-class function $\bar{\beta}$ such that

$$\begin{aligned}\|(s, \tilde{\mathrm{x}})(t)\| \leq{}& \bar{\beta}(\|(s, \tilde{\mathrm{x}})(t_0)\|, t - t_0) \\ &+ c'\mu\gamma_t(\|e\|_{t_0,t} + \|\xi_e\|_{t_0,t})\max\{L, 1\}.\end{aligned} \tag{41}$$

Since $\gamma_t(\|p\|) = c\max\{\|p\|^2, \|^r w\|_\infty \|p\|^5\}$, (40) holds in the domain where $\|p\| < \rho^\star$. Besides, we deduce from (35) and Property 1 that $(p, \tilde{p}_t)$ is ISS with respect to e and ξ_e. Finally, (32) says that e is ISS with respect to ε, so by standard cascade ISS arguments, $(p, \tilde{p}_t)$ is ISS with respect to ε and ξ_e, and we obtain (33).

Authorized licensed use limited to: Universita degli Studi di Roma La Sapienza. Downloaded on July 13,2023 at 11:03:08 UTC from IEEE Xplore. Restrictions apply.

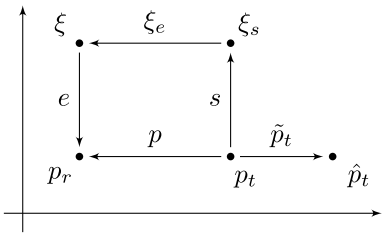

Fig. 5. Error definitions.

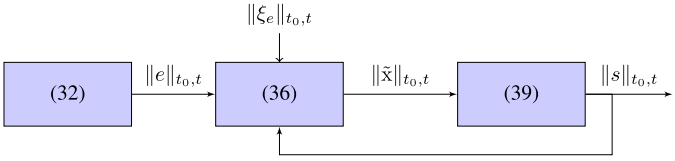

Fig. 6. Interconnections between systems e, s, and $\tilde{\mathrm{x}}$.

VI. Simulation Results

A. Simulator Description

The simulator is implemented following the scheme of Fig. 4, and it is based on real data, collected in field test campaigns, which complete the base model. Indeed, despite that the magnetic dipole represents a good model for the ARVA signal, the characterization of the noise ${}^r w$ as a stochastic variable, of a random white process, required the determination of its statistical properties. The ARVA noise, ${}^r w(t)$, has been defined as a randomly oriented vector whose magnitude and attitude are generated using band-limited with the noise blocks. In particular, the magnitude of the noise is bounded by $\|{}^r w\|_\infty \leq \bar{w} := (2\pi \|p_{\text{eq}}\|^3)^{-1}$ with $\|p_{\text{eq}}\| = 80$ m. This value has been identified after a field test campaign that was performed by measuring the relative position of the receiver with respect to the transmitter (by means of GPS receivers), their relative attitude (by means of inertial measurement units) and the ARVA data. The maximum environment-induced EMI is estimated to be equivalent to an ARVA signal emitted by a transmitter approximately located 80 m far from the receiver. Furthermore, the algorithm implementation into the UAV flight control unit (PixHawk) has been tested in a dedicated software-in-the-loop system, also comprehensive of the ARVA simulator [30].

The relevant control parameters are $K = 1$ and $f_{s,\max} = 0.5$ m/s, whereas the RLS algorithm is characterized by the forgetting factor $\rho = 1$. The excitation trajectory $\xi_e = \text{col}(\xi_{e_1}, \xi_{e_2}, \xi_{e_3})$ is designed with $\xi_{e_i} = A_i \sin(\omega_i t)$, $i = 1, 2, 3$, with $A_1 = A_2 = A_3 = 2$ m and $\omega_1 = 0.7\,2\pi$, $\omega_2 = \omega_1/2$, and $\omega_3 = \omega_1/4$ rad/s. The parameters of the reference trajectory, $f_{s,\max}$, A_i, and ω_i, have been chosen in agreement with the limitations on the maximum speed of 6 m/s. The simulations assume that the center of the inertial reference system (which is defined by the user) coincides with the initial position of the drone, i.e., $p_r(0) = 0$. At time $t = 0$, also the reference trajectory ξ_s is set to be null, thus leading to $\xi_s(0) = 0$, whereas the position of the transmitter is randomly generated to belong to a sphere of radius equal to 50 m, centered at the origin of the inertial space. The maximum initial distance of 50 m has been selected by the following practical experiments that validated the maximum ratings declared in the datasheets of the popular ARVA devices [31], [32]. It is worth noting that, for longer distances, the ARVA signal-to-noise ratio would be too small for letting the algorithm working properly. In particular, the simulations are obtained with $p_t = \text{col}(-32.8, 27.0, 8.6)$ m. The mass of the drone is set to 1 kg, whereas the inertia matrix is $J = \text{diag}(0.1,\ 0.1,\ 0.2)\ \text{kg}\,\text{m}^2$.

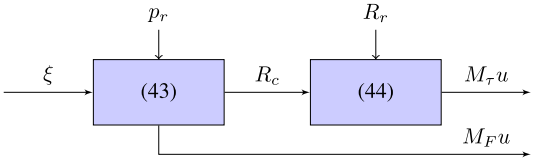

Fig. 7. Stabilizer architecture.

Finally, the simulator has been implemented in a MATLAB/Simulink model with the simulator solver set to integrate the continuous-time ordinary differential equations with an explicit fourth-order solver (ode45 Dormand-Prince), exploiting a variable step size upper bounded by 1 ms.

As for the stabilizer design, we followed the inner–outer design paradigm presented in [28] and shown in Fig. 7. With the position and speed tracking errors defined as

$$\tilde{\mathbf{p}} := \begin{bmatrix} e \\ \dot{\tilde{p}} \end{bmatrix} := \begin{bmatrix} p_r - \xi \\ \dot{p}_r - \dot{\xi} \end{bmatrix} \tag{42}$$

the controller takes the form

$$R_c e_z M_F u = a_c \tag{43}$$

$$\begin{aligned} M_\tau u = {} & J R_r^\top \dot{\omega}_c - k_p \tilde{\epsilon} \\ & - (S(J\tilde{\omega}_c) + k_d)\big(\omega - R_r^\top (R_c^\top \dot{R}_c)^\vee\big) \end{aligned} \tag{44}$$

where $\|R_c e_z M_F u\| = \|u\| = \|a_c\|$ and

$$a_c = -m(g - \ddot{\xi}) + \lambda_2 \text{sat}\left(\frac{k_2}{\lambda_2}\left(\dot{\tilde{p}} + \lambda_1 \text{sat}\left(\frac{k_1}{\lambda_1} e\right)\right)\right)$$

and $\omega_c = R_r^\top (R_c^\top \dot{R}_c)^\vee$ is the desired angular speed, $\tilde{\varepsilon}$ represents the vector part of the quaternion associated with $\tilde{R} = R_c^\top R_r$, and R_c is the desired rotation matrix defined such that $R_c e_z = (a_c/\|a_c\|)$ with the entry $R_c(2, 1) = 0$.

The stabilizer (43) and (44) has been implemented with $k_1 = 0.1$, $k_2 = 15$, $\lambda_1 = 5$, and $\lambda_2 = 15$. Moreover, the saturation functions are defined as $\text{sat}(\cdot) : \mathbb{R}^3 \to \mathbb{R}^3$ that for $n = 1$ is specialized as

$$\text{sat}(s) = \begin{cases} s, & |s| < 1 \\ \text{sign}(s), & |s| \geq 1. \end{cases}$$

For the case $n = 3$, the function is intended to hold componentwise. With these settings, the tracking error e is upper bounded by $\epsilon = 0.5$ m.

B. Result Comments

Fig. 8 shows the trajectory of the receiver with respect to the transmitter and Fig. 9 shows the estimation $\hat{p}_t$. The initial estimation is poor due to the long relative distance from the receiver to the transmitter, which makes the ARVA data particularly noisy. After about 10 s, the identifier collects

Authorized licensed use limited to: Universita degli Studi di Roma La Sapienza. Downloaded on July 13,2023 at 11:03:08 UTC from IEEE Xplore. Restrictions apply.

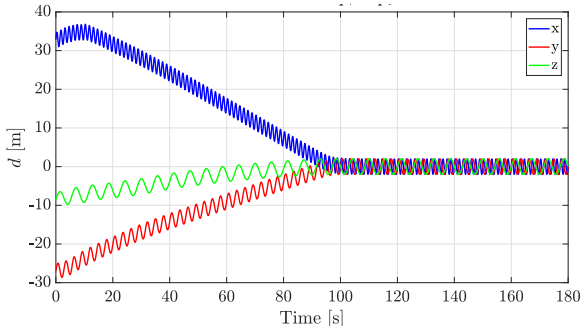

Fig. 8. Distance p from the transmitter to the receiver.

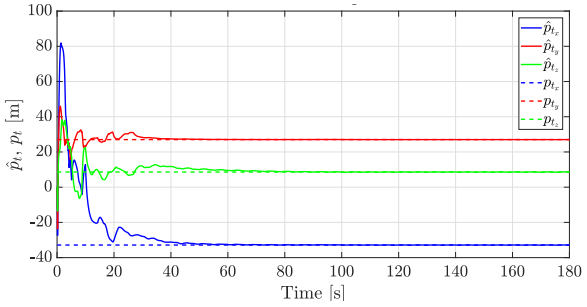

Fig. 9. Estimate of the victim position $\hat{p}_t$.

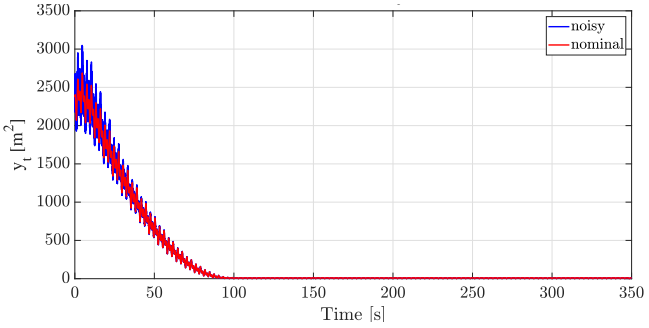

Fig. 10. Effects of the noise ν_t on the ARVA data: comparison with the nominal output.

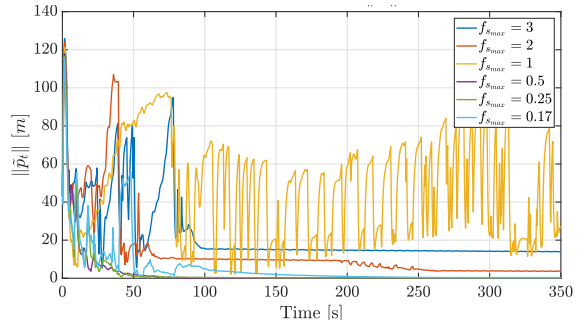

Fig. 11. Comparison of the estimation error $\tilde{p}_t$ with different values of $f_{s,\max}$.

data rich enough to estimate more accurately the transmitter position. Due to the double time scale (guaranteed by small $f_{s,\max}$) between the identifier (faster) and the reference trajectory (slower), the receiver is slowly driven toward the estimated transmitter position, which rapidly converges to the right value. On the other hand, the estimation gets more and more accurate as far as the receiver is close to the

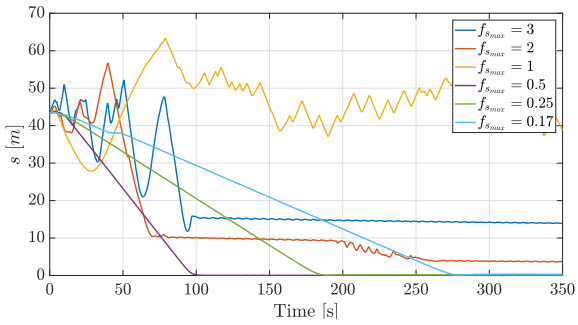

Fig. 12. Comparison of the distance s with different values of $f_{s,\max}$.

transmitter. The effect of the noise ν_t is shown in Fig. 10 where the nominal ARVA output is superposed to the noisy one. We observe that the noise disappears as the receiver approaches the transmitter. It is important to note that a reliable estimate of the victim's position is obtained before the receiver reaches the victim, which constitutes a significant advantage with respect to extremum-seeking techniques.

The choice of $f_{s,\max}$ influences the stability of the overall control scheme (in agreement with the theoretical result). In particular, Figs. 11 and 12 show how the trajectories of the estimation error $\tilde{p}_t$ and the distance $\xi_s - p_t$ change with respect to the variation of $f_{s,\max}$. A reduction of $f_{s,\max}$ leads to a more conservative satisfaction of the stability criterion but makes the receiver staying longer in the noisier zone. As a consequence, the estimation of the transmitter position provided by the identifier is less accurate. Vice versa, higher values of $f_{s,\max}$ induce the receiver to move faster toward the less noisy zone but satisfy in a less conservative way the stability. For this reason, the parameter $f_{s,\max}$ is subject to a design compromise between stability and performance.

VII. Conclusion and Future Works

This article presented an identification scheme for the problem of automatic estimation of the position of avalanche victims who wearing an electromagnetic transmitter (commercially known as ARVA). Due to the peculiar properties of the output map associated with the ARVA receiver, rigidly attached to a quadcopter, the identification process provided by the implementation of an RLS algorithm does not provide the best performance if not supported by a control system that steers the receiver toward the transmitter. The effectiveness of the proposed control scheme was tested in simulations. Future works will regard the real implementation of the proposed strategy on the drones developed in the AirBorne European project (targeting a TRL8 aerial platform).

References

[1] C. Sampedro, A. Rodriguez-Ramos, H. Bavle, A. Carrio, P. de la Puente, and P. Campoy, "A fully-autonomous aerial robot for search and rescue applications in indoor environments using learning-based techniques," *J. Intell. Robotic Syst.*, vol. 95, no. 2, pp. 601–627, Aug. 2019.

[2] D. Falanga, K. Kleber, S. Mintchev, D. Floreano, and D. Scaramuzza, "The foldable drone: A morphing quadrotor that can squeeze and fly," *IEEE Robot. Autom. Lett.*, vol. 4, no. 2, pp. 209–216, Apr. 2019.

[3] S. Waharte and N. Trigoni, "Supporting search and rescue operations with UAVs," in *Proc. Int. Conf. Emerg. Secur. Technol.*, Sep. 2010, pp. 142–147.

Authorized licensed use limited to: Universita degli Studi di Roma La Sapienza. Downloaded on July 13,2023 at 11:03:08 UTC from IEEE Xplore. Restrictions apply.

[4] T. Tomic *et al.*, "Toward a fully autonomous UAV: Research platform for indoor and outdoor urban search and rescue," *IEEE Robot. Autom. Mag.*, vol. 19, no. 3, pp. 46–56, Sep. 2012.
[5] M. A. Goodrich *et al.*, "Supporting wilderness search and rescue using a camera-equipped mini UAV," *J. Field Robot.*, vol. 25, nos. 1–2, pp. 89–110, Jan. 2008.
[6] J. Cacace, A. Finzi, V. Lippiello, M. Furci, N. Mimmo, and L. Marconi, "A control architecture for multiple drones operated via multimodal interaction in search & rescue mission," in *Proc. IEEE Int. Symp. Saf., Secur., Rescue Robot. (SSRR)*, Oct. 2016, pp. 233–239.
[7] J. Cacace, A. Finzi, and V. Lippiello, "Implicit robot selection for human multi-robot interaction in search and rescue missions," in *Proc. 25th IEEE Int. Symp. Robot Human Interact. Commun. (RO-MAN)*, Aug. 2016, pp. 803–808.
[8] G. Bevacqua, J. Cacace, A. Finzi, and V. Lippiello, "Mixed-initiative planning and execution for multiple drones in search and rescue missions," in *ICAPS*, 2015, pp. 315–323.
[9] L. Marconi *et al.*, "The SHERPA project: Smart collaboration between humans and ground-aerial robots for improving rescuing activities in alpine environments," in *Proc. IEEE Int. Symp. Saf., Secur., Rescue Robot. (SSRR)*, Nov. 2012, pp. 1–4.
[10] *Aerial Robotic Technologies for Professional Search and Rescue*. Accessed: Sep. 5, 2020. [Online]. Available: https://www.airborne-project.eu/
[11] E. Bregu, N. Casamassima, D. Cantoni, L. Mottola, and K. Whitehouse, "Reactive control of autonomous drones," in *Proc. 14th Annu. Int. Conf. Mobile Syst., Appl., Services (MobiSys)*, 2016, pp. 207–219.
[12] M. Silvagni, A. Tonoli, E. Zenerino, and M. Chiaberge, "Multipurpose UAV for search and rescue operations in mountain avalanche events," *Geomatics, Natural Hazards Risk*, vol. 8, no. 1, pp. 18–33, Jan. 2017.
[13] M. Grauwiler and L. Oth, "Alcedo–the flying avalanche transceiver," *Zurich: Eur. Satell. Navigat. Competition*, to be published.
[14] J. Cochran and M. Krstic, "Source seeking with a nonholonomic unicycle without position measurements and with tuning of angular velocity Part I: Stability analysis," in *Proc. 46th IEEE Conf. Decis. Control*, Dec. 2007, pp. 6009–6016.
[15] J. Cochran, A. Siranosian, N. Ghods, and M. Krstic, "Source seeking with a nonholonomic unicycle without position measurements and with tuning of angular velocity—Part II: Applications," in *Proc. 46th IEEE Conf. Decis. Control*, Dec. 2007, pp. 1951–1956.
[16] J. Cochran, N. Ghods, and M. Krstic, "3D nonholonomic source seeking without position measurement," in *Proc. Amer. Control Conf.*, Jun. 2008, pp. 3518–3523.
[17] C. G. Mayhew, R. G. Sanfelice, and A. R. Teel, "Robust source-seeking hybrid controllers for nonholonomic vehicles," in *Proc. Amer. Control Conf.*, Jun. 2008, pp. 2722–2727.
[18] C. Mellucci, P. P. Menon, C. Edwards, and P. Challenor, "Source seeking using a single autonomous vehicle," in *Proc. Amer. Control Conf. (ACC)*, Jul. 2016, pp. 6441–6446.
[19] P. A. Ioannou and J. Sun, *Robust Adaptive Control*. Chelmsford, MA, USA: Courier Corporation, 2012.
[20] R. Mehra, "Optimal input signals for parameter estimation in dynamic systems-survey and new results," *IEEE Trans. Autom. Control*, vol. 19, no. 6, pp. 753–768, Dec. 1974.
[21] V. V. Fedorov, *Theory of Optimal Experiments*. Amsterdam, The Netherlands: Elsevier, 2013.
[22] G. C. Goodwin and R. L. Payne, *Dynamic System Identification: Experiment Design and Data Analysis*. New York, NY, USA: Academic, 1977.
[23] M. Zarrop, *Optimal Experiment Design for Dynamic System Identification* (Lecture Notes in Control and Information Sciences), vol. 21. Berlin, Germany: Springer, 1979, doi: 10.1007/BFb0040988.
[24] P. Pinies and J. D. Tardos, "Fast localization of avalanche victims using sum of Gaussians," in *Proc. IEEE Int. Conf. Robot. Autom. (ICRA)*, May 2006, pp. 3989–3994.
[25] N. Ayuso, J. A. Cuchi, F. Leral, and J. L. Villarroel, "Avalanche beacon magnetic field calculations for rescue techniques improvement," in *Proc. IEEE Int. Geosci. Remote Sens. Symp.*, Jul. 2007, pp. 722–725.
[26] K. Reif, F. Sonnemann, and R. Unbehauen, "An EKF-based nonlinear observer with a prescribed degree of stability," *Automatica*, vol. 34, no. 9, pp. 1119–1123, Sep. 1998.
[27] G. Besançon, *Nonlinear Observers and Applications*, vol. 363. Berlin, Germany: Springer, 2007, doi: 10.1007/978-3-540-73503-8.
[28] R. Naldi, M. Furci, R. G. Sanfelice, and L. Marconi, "Robust global trajectory tracking for underactuated VTOL aerial vehicles using inner-outer loop control paradigms," *IEEE Trans. Autom. Control*, vol. 62, no. 1, pp. 97–112, Jan. 2017.
[29] A. Isidori, *Nonlinear Control Systems*. London, U.K.: Springer, 1995, doi: 10.1007/978-1-84628-615-5.
[30] J. Cacace, N. Mimmo, and L. Marconi, "An ARVA sensor simulator," in *Robot Operating System (ROS)* (Studies in Computational Intelligence), vol. 895, A. Koubaa, Ed. Cham, Switzerland: Springer, 2021, doi: 10.1007/978-3-030-45956-7_8.
[31] *Arva Ortovox 3+ User Manual*, Ortovox, Taufkirchen, Germany, May 2019.
[32] *Arva Mammut Barryvox User Manual*, Mammut, Seon, Switzerland, May 2019.

Nicola Mimmo graduated in aerospace engineering from the University of Bologna, Bologna, Italy, in 2009, and the Ph.D. degree in automation from the University of Bologna, in 2015.

Since 2010, he has been working with the Department of Electrical, Electronic, and Information Engineering "Guglielmo Marconi," University of Bologna, on national and European projects for the development of unmanned aerial vehicles for civil applications. He worked with the major national and European aircraft companies for the development of both flight systems and flight control laws that are currently protected by international patents. He is a coauthor of tens of scientific articles. His research interest range from fault-tolerant controls to nonlinear control systems in aerospace.

Dr. Mimmo has organized technical sessions of international conferences.

Pauline Bernard graduated in applied mathematics from MINES ParisTech, Paris, France, in 2014, and the Ph.D. degree in mathematics and control from PSL University in 2017.

She joined the Systems and Control Center, MINES ParisTech. As a Post-Doctoral Scholar, she then visited the Hybrid Systems Laboratory, University California at Santa Cruz, Santa Cruz, CA, USA, and the Center for Research on Complex Automated Systems, University of Bologna, Bologna, Italy. In 2019, she became an Assistant Professor at the Systems and Control Center, MINES ParisTech, PSL University. Her research interest includes the observation and output regulation of nonlinear and hybrid systems.

Dr. Bernard received the European Ph.D. Award on Control for Complex and Heterogeneous Systems for her work on observer design for nonlinear systems in 2018.

Lorenzo Marconi (Fellow, IEEE) graduated in electrical engineering from the Department of Electronics, Computer Science and Systems, University of Bologna, Bologna, Italy, in 1995. He received the Ph.D. degree from the Department of Electronics, Computer Science and Systems, University of Bologna, in 1998.

Since 1999, he has been an Assistant Professor with the Department of Electronics, Computer Science and Systems, University of Bologna, where he is currently a Full Professor. He is a coauthor of more than 250 technical publications on the subject of linear and nonlinear feedback designs published on international journals, books, and conference proceedings.

Dr. Marconi is a fellow of the IEEE for contributions to feedback design of nonlinear systems and unmanned aerial vehicles. He received the Outstanding Application Paper Award from IFAC for a coauthored paper published on *Automatica* in 2005. He was a co-recipient of the 2014 IEEE Control Systems Magazine Outstanding Paper Award for the best paper published in the magazine and the 2018 O. Hugo Schuck Best Paper Award.

Authorized licensed use limited to: Universita degli Studi di Roma La Sapienza. Downloaded on July 13,2023 at 11:03:08 UTC from IEEE Xplore. Restrictions apply.